Optica Applicata, Vol. XLV, No. 2, 2015
DOI: 10.5277/oa150203

Polarization dependence of patterning effects in quantum well semiconductor optical amplifier-based wavelength conversion

CUI QIN[1*], WEIKANG SHEN[1], JING ZHAO[1], HUILONG YU[1], ENMING XU[2]

[1]School of Communication Engineering, Nanjing Institute of Technology, Nanjing, 211167, China

[2]School of Optoelectronic Engineering, Nanjing University of Posts and Telecommunications, Nanjing 210023,China

[*]Corresponding author: cuiqincui@gmail.com

In this paper, polarization dependence of patterning effects in quantum well semiconductor optical amplifier-based wavelength conversion is experimentally and theoretically investigated. The carrier and photon density rate equations are numerically solved by using the time-domain traveling wave model. The material gain calculation, including the strain effect in the active layer, is based on the **k**·**p** method. By comparing experimental and computational results, it is demonstrated that the polarization of the injection signal has a significant influence on the gain recovery time of quantum well semiconductor optical amplifier. Under the cross-polarized signals injection, the output signals suffer the weakest and strongest patterning effects both for unstrained and tensile strained quantum well semiconductor optical amplifiers.

Keywords: semiconductor optical amplifiers, polarization, patterning effect.

1. Introduction

Semiconductor optical amplifiers (SOAs) have been exploited to realize many all-optical signal processing applications due to their compactness, direct current pumping, wide gain spectrum and various nonlinearities advantages [1, 2]. Wavelength conversion is one of SOA's important applications in wavelength division multiplexed (WDM) systems. Recently, error-free 320 Gb/s wavelength conversion by employing a SOA has been demonstrated [3]. At very high operation speed, SOAs' applications are severely limited due to the slow gain recovery, causing unwanted patterning effect in the converted signals [4]. The patterning effect is a main factor for output signal's per-

formance, especially in those schemes based on cross-gain modulation (XGM) and cross-phase modulation (XPM).

Polarization sensitivity of the optical gain in SOAs has attracted a lot of attention recently, although the physical mechanisms of the operation are still under intensive research [5, 6]. Many researches focus on the influence of polarization on the gain spectrum and the nonlinear polarization rotation effect [7, 8]. There are few studies on the impact of polarization on the patterning effect in wavelength conversion based on XGM. The gain and refractive index differences between TE and TM modes have evident effects on gain and phase recovery process. Therefore the patterning effects in QW SOA-based wavelength conversion are strongly dependent on the polarization states. Polarization dependence in SOAs is an issue that needs to be addressed to improve their performance. The goal of this paper is to improve the quality of the output eye diagram by finding suitable input polarization states of the probe and pump lights.

In this paper, we present a detailed study on the polarization properties of patterning effects in QW SOA-based wavelength conversion. First, the polarization dependence of wavelength conversion based on QW SOA is experimentally investigated. Then, the gain and refractive index change values of TE and TM modes in rate equations are obtained by the parabolic band model and $\mathbf{k}\cdot\mathbf{p}$ method. Thus, the effect of the band structure of SOA on the patterning effects occurred in wavelength conversion and can be analyzed in our theoretical model. The comparisons of gain and phase recovery for different polarize signals injected into the lattice-matched and tensile strained QW SOAs are analyzed. Finally, the patterning effects in wavelength conversion based on the unstrained and tensile strained QW SOAs are compared. It demonstrated that the polarization of the injection signal has a significant influence on patterning effects. Thus, in order to obtain high quality output signal, the polarization of the injection signal needs to be chosen carefully.

The paper is organized as follows: Section 2 analyzes the results of wavelength conversion experiment for different polarizations of the injection signal; Section 3 describes the traveling wave rate equation model for characterizing the behavior of the SOA; Section 4 discusses the results of the simulation; conclusions are given in Section 5.

2. Experimental setup and results

Figure 1 shows the experimental setup. A mode-locked semiconductor laser is used to generate 10 GHz, 2.5 ps pluses at around 1556.40 nm. A laser source emits a continuous wave (CW) probe beam at a wavelength of 1546.94 nm. After passing through the erbium doped fiber amplifier (EDFA), the attenuator (ATT) and the polarisation controller (PC), the pump signal combined with the CW lights by a polarization beam combiner (PBC). The EDFAs and the ATTs are used to assure the lights that enter the SOA have low intensities. The average optical powers of probe and pump are 3 and 5 dBm, respectively. The PC1 and PC2 are used to adjust the polarization of the input

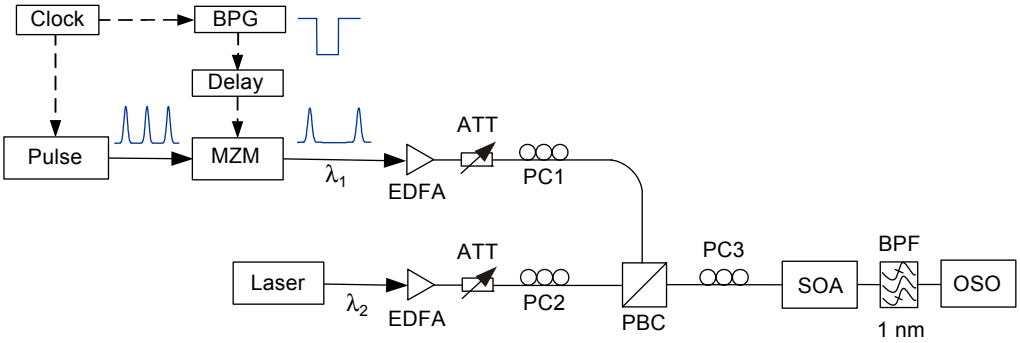

Fig. 1. Schematic diagram of experimental setup. BPG – bit pattern generator, MZM – Mach–Zehnder modulator, EDFA – erbium doped fiber amplifier, ATT – attenuator, PC – polarisation controller, PBC – polarization beam combiner, SOA – semiconductor optical amplifier, BPF – band-pass filter, OSO – optical sampling oscilloscope.

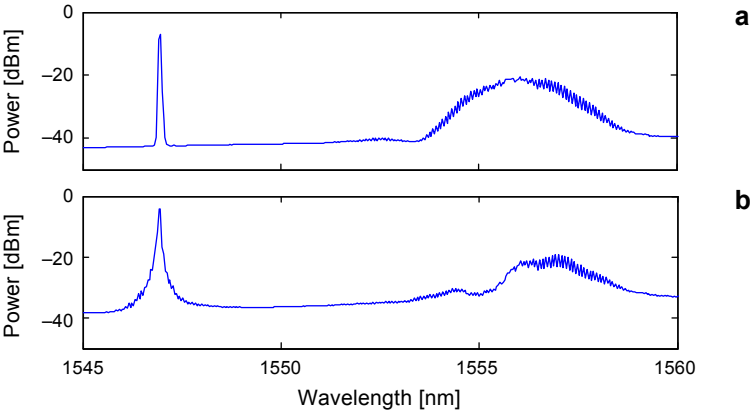

Fig. 2. Optical spectrum of SOA input signals (**a**) and optical spectrum of SOA output signal (**b**).

signals to the TE and TM polarizations of the PBC. The PC3 is used to adjust the polarizations of the input signals to the orientations of the QW SOA layers. The output channel of probe is selected by an optical filter.

The spectra of SOA input signals and output signals are plot in Fig. 2. When the signals are fed into the SOA, the spectrum of CW light is significantly broadened due to XGM and XPM effects in the active region of the QW SOA.

The eye diagrams for a cross-polarized case are plotted in Fig. 3. According to the adjustment of the PC3, the worst and the best quality eye diagram are obtained in Figs. 3**a** and 3**b**, respectively. In Figure 3**b**, the eyelid of the eye diagram is the narrowest and the eye opening is the widest. In this case, the pattern effect is smaller than in the other case. It is more suitable to be used in wavelength conversion, and improve the quality of the output signal. Although TE or TM mode cannot be distinguished in

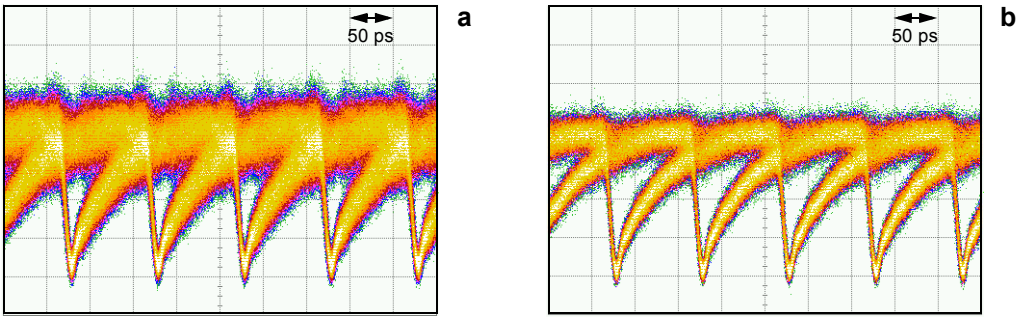

Fig. 3. Eye diagrams of the probe light after band pass filter (see text for explanation).

our experiment, it demonstrated that the polarization states of the probe and pump lights have influence on the patterning effects in wavelength conversion. The detailed theoretical investigation is presented below.

3. Numerical model

The SOAs' behaviors are characterized through the traveling wave rate equation model including ultrafast effects. We only consider the forward propagating signals and neglect the reverse signals. To fully describe the propagation of a pulse inside the SOAs, the rate equations for carrier density, photon density and phase are as follows [9]:

$$\frac{\mathrm{d}N}{\mathrm{d}t} = \frac{I}{qV} - R(N) - \sum_i v_g \frac{g_i^{\mathrm{TE/TM}}}{1+\varepsilon_{\mathrm{sh}} S^{\mathrm{TE/TM}}} S^{\mathrm{TE/TM}} \tag{1}$$

$$\frac{\partial S_i^{\mathrm{TE/TM}}}{\partial z} + \frac{1}{v_g}\frac{\partial S_i^{\mathrm{TE/TM}}}{\partial t} = \left(\Gamma^{\mathrm{TE/TM}} \frac{g_i^{\mathrm{TE/TM}}}{1+\varepsilon_{\mathrm{sh}} S_i^{\mathrm{TE/TM}}} - \alpha_{\mathrm{tot},\,i} \right) S_i^{\mathrm{TE/TM}} \tag{2}$$

$$\frac{\partial \varphi_i}{\partial z} + \frac{1}{v_g}\frac{\partial \varphi_i}{\partial t} = -\Gamma^{\mathrm{TE/TM}} \frac{\omega}{c} (-\delta n^{\mathrm{TE/TM}} + \delta n_p) \tag{3}$$

where I is the injected current, V is the active volume, $R(N) = AN + BN^2 + CN^3$, A is the nonradiative recombination coefficient, B is the bimolecular recombination coefficient and C is the Auger recombination coefficient; q is the magnitude of a unit charge; v_g is the group velocity, ω is the optical frequency, c is the speed of light in vacuum; the subscript $i = 1, 2$ denotes the pump signal and probe signal, respectively; Γ and α_{tot} are waveguide confinement factor and waveguide loss, respectively; $\Gamma^{\mathrm{TE}} = 0.2$ and $\Gamma^{\mathrm{TM}} = 0.14$. The superscripts TE and TM denote the polarization directions of input signals. In Eq. (3), δn_p describing the band-to-band refractive

index-change can be obtained from [10]; ε_{sh} is the nonlinear gain coefficient due to spectral hole burning

$$\varepsilon_{\text{sh}} = \frac{\omega |d_k|^2 (\tau_{1c} + \tau_{1v}) \tau_2 v_g}{\varepsilon_0 n_r c \hbar} \tag{4}$$

where τ_{1c} and τ_{1v} are the intraband carrier–carrier scattering time constants, τ_2 is the relaxation time of the dipole, ε_0 is the permittivity in vacuum, n_r is the refractive index of the material, and d_k is the dipole moment of the transition [11]

$$|d_k|^2 = \frac{q^2}{6 m_0 \omega^2} \left(\frac{m_0}{m_c} - 1 \right) \frac{E_g (E_g + \Delta_0)}{E_g + \frac{2\Delta_0}{3}} \tag{5}$$

where m_0 is the free-electron mass, m_c is the electron effective mass, Δ_0 is the spin-orbit splitting, and E_g is the gap energy.

The conduction and valence band structures of the QW SOA are obtained by the parabolic band model. For the valence band, the Hamiltonian for the valence envelope wave functions is derived by Luttinger and Kohn using **k**·**p** method [12, 13]. The semiconductor material gain and refractive index change can be obtained from the imaginary part and real part of the frequency domain susceptibility [14]

$$\tilde{\chi}(\omega) = \frac{\tilde{P}}{\varepsilon_0 \tilde{E}(z)} = \\ = -\frac{1}{\varepsilon_0 \hbar \gamma V} \sum_k |\boldsymbol{\mu}_k|^2 \left[f_n^c(k) - f_{\sigma m}^v(k) \right] L(\omega_k - \omega) \left(\frac{\omega_k - \omega}{\gamma} + j \right) \tag{6}$$

where

$$f_n^c(k) = \left[1 + \exp\left(\frac{E_n^c(k) - E_{fc}}{k_B T} \right) \right]^{-1} \tag{7}$$

$$f_{\sigma m}^v(k) = \left[1 + \exp\left(\frac{E_{\sigma, m}^v(k) - E_{fv}}{k_B T} \right) \right]^{-1} \tag{8}$$

$$E_{\sigma, nm}^{cv}(k) = E_n^c(k) - E_{\sigma, m}^v(k) \tag{9}$$

where $L(\omega_k - \omega)$ is the Lorentzian line-shape function, γ is the half linewidth of the Lorentzian function, $\boldsymbol{\mu}_k$ is the momentum matrix element, $f_n^c(k)$ and $f_{\sigma m}^v(k)$ are the Fermi–Dirac distribution functions for the n-th subband in the conduction band and

the m-th subband in the valence band, E_{fc} and E_{fv} are the quasi-Fermi levels for electrons and holes, respectively.

All equations involved in the calculation are solved numerically. The numerical model is based on the polarized optical field having indirect interaction via the carriers in a polarization SOA. The distributions of carriers, photon densities and phase are simulated by dividing the SOA into many sections along the longitudinal direction. The material gain is linked to the carrier density through the quasi-Fermi level.

4. Results and discussion

Based on the above numerical and theoretical model, the polarization dependence of patterning effects in QW SOA-based wavelength conversion was simulated in this section. In this paper, the current is set at 200 mA. The pump and probe wavelengths are fixed at 1552 and 1550 nm, respectively. The probe signal is 1 mW continues wave. The pump signal is Gaussian pulse with 2 ps FWHM pulse width and 10 mW peak power at 80 Gb/s. The legends in the below figures $i_{\mathrm{pu}}\, j_{\mathrm{pr}}$ represent that the pump signal is i polarization and the probe signal is j polarization.

The results of lattice-matched QW SOA are shown in Fig. 4. The gain compression for the TE polarize pump signal is larger than that for the TM polarize pump signal. The maximum total gain compression and the maximum phase change are achieved in $\mathrm{TE_{pu}TM_{pr}}$ case. At the same time, the minimum gain compression and the minimum phase change are achieved in $\mathrm{TM_{pu}TE_{pr}}$ case. When the pump and probe are co-polarization, the total gain compressive, recovery process and the phase change are about the same. The fast gain recovery is evident for $\mathrm{TM_{pu}TE_{pr}}$ case, where only a small level of slow gain recovery remains. The fast gain recovery process is weak for $\mathrm{TE_{pu}TM_{pr}}$ case which needs the longest time to full recovery. It is indicated that the spectral hole burning (SHB) and carrier heating (CH) effects made a great contribution to the fast recovery component for $\mathrm{TM_{pu}TE_{pr}}$ case.

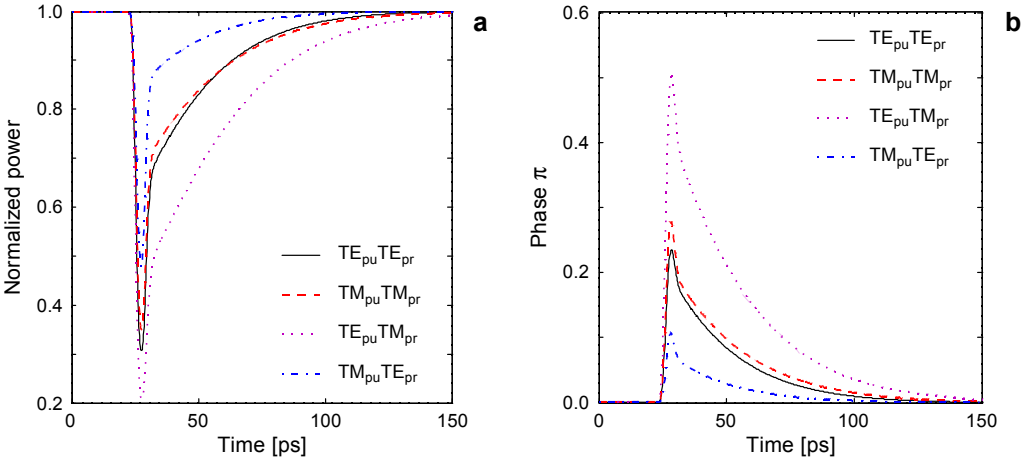

Fig. 4. Gain (**a**) and phase (**b**) dynamics of lattice-matched QW SOA.

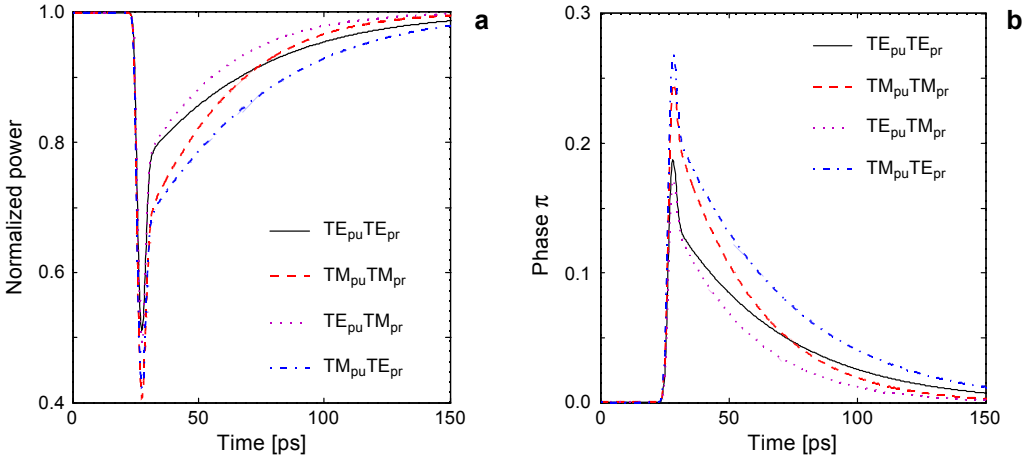

Fig. 5. Gain (**a**) and phase (**b**) dynamics of the tensile strained QW SOA.

Figure 5 shows the comparison of gain and phase recovery for different polarize signals injected into the tensile strained QW SOA. When the pump signal is TM polarization, the gain recovery curve shows deeper gain compression and stronger phase change magnitude. The contrary results are obtained by injecting TE polarize pump signal. The 90% gain recovery time is shorter for TM polarize probe light than that for TE polarize probe light. Comparing the four polarization configurations, the tensile strained QW SOA has the fastest gain recovery speed for $TE_{pu}TM_{pr}$ case and the longest recovery time for $TM_{pu}TE_{pr}$ case. It is demonstrated that the SHB and CH ultrafast effects and interband recombination process are enhanced for $TE_{pu}TM_{pr}$ configuration in the tensile strained QW SOA.

The reason behind our simulation phenomenon may be explained with the help of the gain spectra which are shown in Fig. 6. The three-dimensional carrier density is 2.5×10^{24} m^{-3}. The TE (TM) gains are plotted in solid (dash) curves. It can be seen clear-

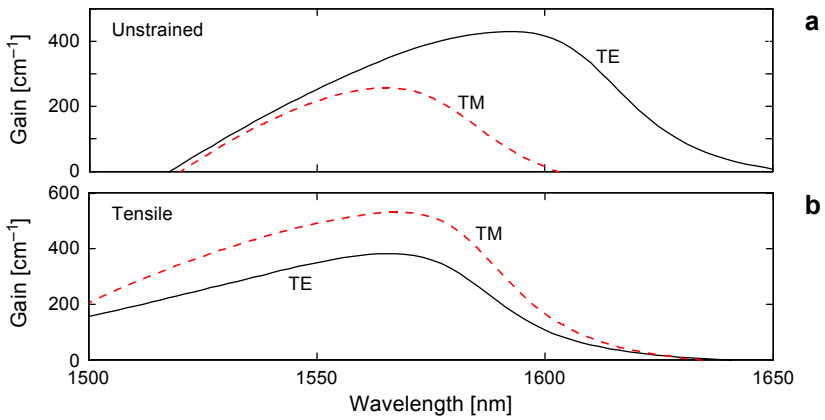

Fig. 6. Gain spectra of the lattice-matched QW SOA (**a**) and tensile strained QW SOA (**b**).

ly that the TE gain is larger than the TM gain for the unstrained QW while the TM gain is larger than the TE gain for the tensile strained QW in the signal wavelength range. When the active region of the SOA is lattice-matched QW, the TE polarize pump signal will obtain more gain than the TM polarize pump signal. So the total gain compression is larger for the TE pump signal in the unstrained QW SOA. Meanwhile, the steady state carrier density is lower for the TE polarize probe signal than that for the TM polarize probe signal. The gain near the output facet can get saturated much easier, which is a benefit for raising the gain recovery speed. Thus, the gain recovery process is faster for the TE polarize probe signal. The results of the tensile strained QW SOA can be also analyzed by the similar theory.

The waveforms and corresponding eye diagrams of the unstrained and tensile strained QW SOAs are plotted in Figs. 7 and 8, respectively. The pump signal is ran-

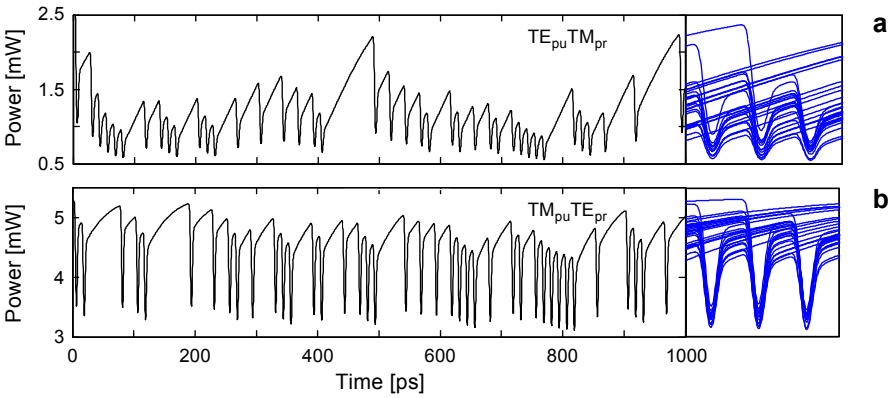

Fig. 7. Waveforms and corresponding eye diagrams of the unstrained QW SOAs for $TE_{pu}TM_{pr}$ configuration (**a**) and $TM_{pu}TE_{pr}$ configuration (**b**).

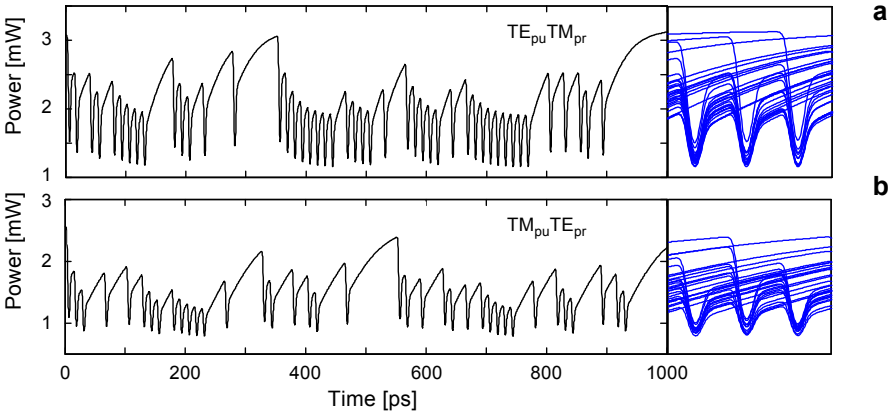

Fig. 8. Waveforms and corresponding eye diagrams of the tensile strained QW SOAs for $TE_{pu}TM_{pr}$ configuration (**a**) and $TM_{pu}TE_{pr}$ configuration (**b**).

dom Gaussian pulses. It is clearly seen that the eyelid of the eye diagram becomes narrow and the eye opening becomes broadened for $TM_{pu}TE_{pr}$ configuration in the unstrained QW SOA. Comparing the eye diagrams in Fig. 8, the quality of the signal is also improved slightly for $TE_{pu}TM_{pr}$ configuration in the tensile strained QW SOA. The polarization configurations, which have short gain recovery time, will show better performance in wavelength conversion based on XGM. This is in agreement with the experimental results to some extent.

5. Conclusion

In this paper, we investigated the polarization dependence of patterning effects in QW SOA-based wavelength conversion. It experimentally and theoretically demonstrated that the polarization states of input signals have a significant impact on the patterning effects. Comparing the results of the gain and phase recovery dynamics in the strained QW SOAs, the gain recovery is accelerated for the $TM_{pu}TE_{pr}$ configuration in the unstrained QW SOA and $TE_{pu}TM_{pr}$ configuration in the tensile strained QW SOAs. These configurations are suitable for XGM. And the patterning effect in wavelength conversion based on XGM is smaller. The phase change is significantly enhanced for $TE_{pu}TM_{pr}$ configuration in the unstrained QW SOA and $TM_{pu}TE_{pr}$ configuration in the tensile strained QW SOA. These configurations are appropriate for XPM. For high-speed optical communications, the appropriate choice of a polarization state will contribute to the excellent performance: in terms of the weaken patterning effect.

Acknowledgements – This work is supported by the National Natural Science Foundation of China (No. 61302026) and the Scientific Research Foundation of Nanjing Institute of Technology (Grant Nos. YKJ201320, YKJ201322 and YKJ201323).

References

[1] Jun Qin, Guo-Wei Lu, Takahide Sakamoto, Kouichi Akahane, Naokatsu Yamamoto, Danshi Wang, Cheng Wang, Hongxiang Wang, Min Zhang, Tetsuya Kawanishi, Yuefeng Ji, *Simultaneous multichannel wavelength multicasting and XOR logic gate multicasting for three DPSK signals based on four-wave mixing in quantum-dot semiconductor optical amplifier*, Optics Express **22**(24), 2014, pp. 29413–29423.

[2] Jing Xu, Xinliang Zhang, Yin Zhang, Jianji Dong, Deming Liu, Dexiu Huang, *Reconfigurable all-optical logic gates for multi-input differential phase-shift keying signals: design and experiments*, Journal of Lightwave Technology **27**(23), 2009, pp. 5268–5275.

[3] Liu Y., Tangdiongga E., Li Z., De Waardt H., Koonen A.M.J., Khoe G.D., Xuewen Shu, Bennion I., Dorren H.J.S., *Error-free 320-Gb/s all-optical wavelength conversion using a single semiconductor optical amplifier*, Journal of Lightwave Technology **25**(1), 2007, pp. 103–108.

[4] Jing Xu, Yunhong Ding, Peucheret C., Weiqi Xue, Seoane J., Zsigri B., Jeppesen P., Mørk J., *Simple and efficient methods for the accurate evaluation of patterning effects in ultrafast photonic switches*, Optics Express **19**(1), 2011, pp. 155–161.

[5] Connelly M.J., *Theoretical calculations of the carrier induced refractive index change in tensile--strained InGaAsP for use in 1550 nm semiconductor optical amplifiers*, Applied Physics Letters **93**(18), 2008, article 181111.

[6] ANTONIADES N., REICHMANN K.C., IANNONE P.P., FRIGO N.J., LEVINE A.M., ROUDAS I., *The impact of polarization-dependent gain on the design of cascaded semiconductor optical amplifier CWDM systems*, IEEE Photonics Technology Letters **18**(20), 2006, pp. 2099–2101.

[7] SHUANG ZHAO, CHONGQING WU, MU CHENG, ZHENGYONG LI, ZHEN FENG, *Poincare sphere method for optimizing the wavelength converter based on nonlinear polarization rotation in semiconductor optical amplifiers*, IEEE Journal of Quantum Electronics **45**(8), 2009, pp. 1006–1013.

[8] SONGNIAN FU, WEN-DE ZHONG, SHUM P., CHONGQING WU, ZHOU J.Q., *Nonlinear polarization rotation in semiconductor optical amplifiers with linear polarization maintenance*, IEEE Photonics Technology Letters **19**(23), 2007, pp. 1931–1933.

[9] DAILEY J., KOCH T., *Simple rules for optimizing asymmetries in SOA-based Mach–Zehnder wavelength converters*, Journal of Lightwave Technology **27**(11), 2009, pp. 1480–1488.

[10] BENNETT B.R., SOREF R.A., DEL ALAMO J.A., *Carrier-induced change in refractive index of InP, GaAs and InGaAsP*, IEEE Journal of Quantum Electronics **26**(1), 1990, pp. 113–122.

[11] JIAN WANG, SCHWEIZER H.C., *A quantitative comparison of the classical rate-equation model with the carrier heating model on dynamics of the quantum-well laser: the role of carrier energy relaxation, electron–hole interaction, and Auger effect*, IEEE Journal of Quantum Electronics **33**(8), 1997, pp. 1350–1359.

[12] CHIH-SHENG CHANG, SHUN LIEN CHUANG, *Modeling of strained quantum-well lasers with spin-orbit coupling*, IEEE Journal of Selected Topics in Quantum Electronics **1**(2), 1995, pp. 218–229.

[13] SHUNJI SEKI, YAMANAKA T., WAYNE LUI, YUZO YOSHIKUNI, YOKOYAMA K., *Theoretical analysis of pure effects of strain and quantum confinement on differential gain in InGaAsP/lnP strained-layer quantum-well lasers*, IEEE Journal of Quantum Electronics **30**(2), 1994, pp. 500–510.

[14] CHOW W.W., *Semiconductor-Laser Physics*, Springer-Verlag, New York, 1994.

Received December 22, 2014
in revised form February 4, 2015